Effect of Stiffness on the Phase Behavior of Cubic Lattice Chains

Michele A. Floriano* and Vanessa Firetto

Dipartimento di Chimica Fisica "F. Accascina", Università di Palermo, Viale delle Scienze, Parco d'Orleans, Ed. 17, 90128 Palermo, Italy

Athanassios Z. Panagiotopoulos

Department of Chemical Engineering, Princeton University, Princeton, New Jersey 08544-5263

Received November 12, 2004; Revised Manuscript Received January 4, 2005

ABSTRACT: Grand canonical Monte Carlo (GCMC) simulations assisted by histogram reweighting techniques were used to study the effect of chain flexibility on the solution phase behavior for cubic lattice short chains with 4−32 segments. This was done by varying gradually a stiffness parameter until the calculated mean end-to-end distance approached the fully extended length. For both flexible and stiff chains it was found that the critical temperature, obtained by mixed-field finite size analysis, increased with chain length and the critical density moved to lower values, in agreement with experimental observations. The extrapolated infinite chain length critical temperature was greater for stiffer chains. This was attributed to the larger number of favorable intermolecular contacts between longer and/or rigid polymer chains. Critical temperatures obtained in this work are in excellent agreement with previous computer simulations and theoretical predictions. It was also found that phase envelopes of flexible chains fell below and within the rigid counterparts. At high densities, long ($r = 16$ and $r = 32$) and rigid chains showed a tendency to form ordered dense structures which were not observed in fully flexible or short chains. By comparing values of the Flory x_1 and x_2 parameters, obtained from fits of the calculated phase diagrams at different degrees of chain stiffness, it was concluded that, when phase separation occurs, packing stiff rods leads to a smaller entropy change and a less endothermic process. The present results support the idea that, in polymeric systems, an increase in the stiffness of the chain backbone is equivalent to an increase in chain length.

Introduction

Polymeric materials are ubiquitous, and they are increasingly important in many applications due to their processability and to the extremely broad range of properties that they exhibit. Their phase behavior is central in almost every aspect of polymer processing. To control the phase behavior, one has available a number of variables, such as temperature and pressure but also polymer molecular architecture.[1−4]

The critical point of phase separation between polymer-rich and polymer-lean phases in polymer solutions has been studied experimentally,[5−10] by theory,[11−15] and by computer simulations for both flexible[16−25] and nonflexible chains.[26−38] Hard-sphere chain equations of state[15] based on statistical mechanics have been developed to describe the behavior of a model of flexible chain molecules of freely jointed hard spherical segments. Despite the rather crude approximations, the properties of these hard-sphere chain models take into account some significant features of real polymer molecules, including segment excluded-volume effects and segment connectivity.

Computer simulations of phase equilibria in lattice models for flexible polymer systems have quite a long history. For example, in previous studies[16,21,22] it has been observed that the critical temperature depends on chain length in a manner consistent with the functional form suggested by the Flory−Huggins theory. Wilding et al.[20] have studied the critical point properties of lattice homopolymers by using the bond fluctuation model. The chain length dependence of the end-to-end distance indicates that the chains are not collapsed at the critical point. However, real polymeric chains exhibit local stiffness due to chemical constraints of rotational and torsional angles. As the local stiffness is increased, intramolecular screening is reduced, and interior sites become much more open to intermolecular contacts. The phase behavior of polymer systems is sensitive to subtle variations in molecular architecture, and thus, systematic investigations in this direction can be very instructive.

To formulate realistic models taking into account the effect of changes in stiffness of actual polymer systems, a large amount of work has been performed during the past decades. Honnell et al.[26] have explored the effects of chain stiffness on the intermolecular structure of homopolymer melts. Sheng et al.[30] have determined vapor−liquid equilibrium diagrams of semiflexible chains. Kumar et al.[29] have investigated the properties of branched and linear polyolefins; the effect of branching was replaced by an effective stiffness parameter that depended on polymer architecture. Blas et al.[33] have studied the phase equilibrium behavior of mixtures of nonassociating chain like molecules and liquid−vapor equilibria of both pure homonuclear and heteronuclear chains by Gibbs ensemble Monte Carlo simulations. For short chains, excellent agreement with Soft-SAFT theory[12] was found. Perera et al.[32] have compared the liquid−gas phase diagram obtained by different computational methods. They concluded that the combination of the Gibbs ensemble simulation method together with Wegner fits yields reliable coexistence data. Lü et al.[37] have performed GCMC simulations of a simple equilibrium polymer model, consisting of hard-sphere monomers reversibly self-assembling into chains of

* Corresponding author. E-mail: flor@unipa.it.

10.1021/ma047671s CCC: $30.25
Published on Web 02/22/2005

arbitrary length, using a novel sampling method to add or remove multiple monomers during a single MC move. Ivanov et al.[36] have studied the dilute−dense and the isotropic−nematic transitions in solutions at different semiflexible polymer concentrations. In the case of semiflexible and rigid polymers, the formation of ordered structures due to the geometric restrictions imposed by their molecular architecture is expected. This is not true for flexible chains. Indeed, Wojciechowski et al.[28] have demonstrated that systems of flexible molecules of tangent spherical segments exhibit an fcc close-packed arrangement of monomers with random bonds but no long-range orientational order between bond vectors.

Although Galindo et al.[38] have obtained the global phase diagrams (i.e., vapor−liquid and fluid−solid equilibria) for three-center and five-center molecules, they consider only two limiting cases: freely jointed chains and linear rigid chains. The influence of gradual stiffness changes on the phase behavior of polymer solutions has not been reported.

The purpose of the present study is to investigate the effect of different degrees of chain stiffness on the phase behavior of model−polymer chains. Histogram reweighting[39] grand canonical Monte Carlo (GCMC) simulations combined with mixed-field finite scaling concepts[40] were used in order to predict the phase coexistence and critical parameters in model polymer−solvent systems. The structure of this paper is as follows. The first section summarizes the model and computational methods used. It is followed by the description of our results for the phase diagrams and critical parameters of chains with varying flexibility, from fully flexible to almost rodlike. In the concluding section, the main findings are summarized and suggestions for future studies are outlined.

Model, Method, and Simulation Details

In this work, homopolymers were modeled as chains of r connected sites on a simple cubic lattice of volume L^3. Periodic boundary conditions were imposed in the x, y, and z directions. Nearest-neighbor pairs of sites interacted along the lattice vectors (0,0,1), (0,1,1), and (1,1,1), and their reflections along the principal axes, resulting in a coordination number $z = 26$. This is a higher coordination number than the commonly used $z = 6$, resulting in significantly more local chain flexibility. The interaction energies between nearest-neighbor pairs are indicated as ϵ_{ps}, ϵ_{pp}, and ϵ_{ss} where the subscript "p" stands for polymer, while "s" denotes the solvent. The only relevant energy scale is

$$\epsilon = 2\epsilon_{ps} - (\epsilon_{ss} + \epsilon_{pp}) \tag{1}$$

The polymer−polymer interaction was set to −1 (resulting in attractive interactions for nearest-neighbor contacts) and the solvent−solvent and polymer−solvent interactions to 0. The reduced temperature, T^*, was defined with respect to the unit of interaction energies as $T^* = kT/\epsilon$, where k is Boltzmann's constant.

Chain stiffness was introduced by adding a bending potential term, U_{bend}, defined by

$$U_{bend} = \alpha(1 + \cos\theta) \tag{2}$$

where θ is the angle between three consecutive beads of the molecular backbone and α is a parameter controlling the stiffness of the chain; $\alpha = 0$ corresponds to a fully flexible chain whereas increasingly larger values make the chains stiffer, all the way to rodlike molecules. The chain stiffness potential together with nearest-neighbor ($z = 26$) attraction and the volume exclusion condition preventing multiple occupancy of any site fully define the energy function of the model. This energy function was used in turn for accepting and rejecting Monte Carlo moves.

Monte Carlo simulations were performed in the grand canonical ensemble, where density and energy, which are also the statistical variables, are allowed to fluctuate in the simulation box while the chemical potential, μ, the volume, V, and the temperature, T, are held fixed. Full details of the simulation method and Monte Carlo moves can be found elsewhere.[21,30] Histogram reweighting was used to estimate phase coexistence results not covered by actual simulations. This approach makes it possible to minimize the number of necessary simulations for a given system.

For a single simulation run, the number of times a particular set of values for the number of particles, N, and the energy, E, that occur is stored as a histogram, $H(N,E)$:

$$H(N,E) = \Omega(N,V,E)e^{-\beta E + \beta\mu N}/\Xi(\mu,V,T) \tag{3}$$

where $\Omega(N,V,E)$ is the microcanonical partition function and $\Xi(\mu,V,T)$ is the grand partition function.

Different simulation runs at chemical potentials and temperatures covering the range of interest were combined using the method of Ferrenberg and Swendsen[39] to obtain an estimate of the microcanonical partition function valid over a broad range of particle numbers and energies. From this function, all thermodynamic properties can be calculated. More details on the computational approach are available in previous publications.[21,30]

Mixed-field finite scaling analysis[40] was applied to determine the critical parameters. Only simulation results obtained in conditions close to the critical region were used, assuming that these data was within the scaling regime. The procedure is outlined below.

The order parameter, M, was defined, combining the number of particles N and energy E, as

$$M = N - sE \tag{4}$$

where s is a nonuniversal "field mixing" parameter.

At the critical point, the normalized probability distribution at a given system size L, $P_L(x)$, assumes a universal shape with

$$x = a_M{}^{-1}L^{\beta/\nu}(M - M_c) \tag{5}$$

The subscript "c" denotes the critical value. The coefficient $a_M{}^{-1}$ was chosen in such a way that the distribution of x, $P_L(x)$, resulted in unit variance. The $P_L(x)$ data were then plotted and compared to the universal fixed form (Ising distribution of the magnetization). In this analysis no pressure mixing in the scaling fields was assumed.[40]

For each system, the temperature, chemical potential, and the field-mixing parameter, s, were adjusted until the order parameter distribution matched that of the universal Ising curve. A simplex search algorithm was applied to find values in the T, μ, and s parameter space

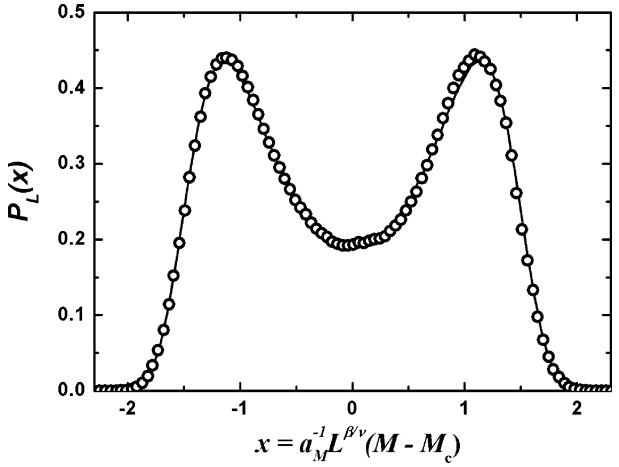

Figure 1. Scaled order parameter distribution, $P_L(x)$, vs the order parameter x. The universal curve for the Ising three-dimensional universality class is indicated by the continuous line (data courtesy of N. Wilding). Simulation points (○) refer to chains of length $r = 8$ at $T_c = 12.45$, $L = 15$, and $\alpha = 250$.

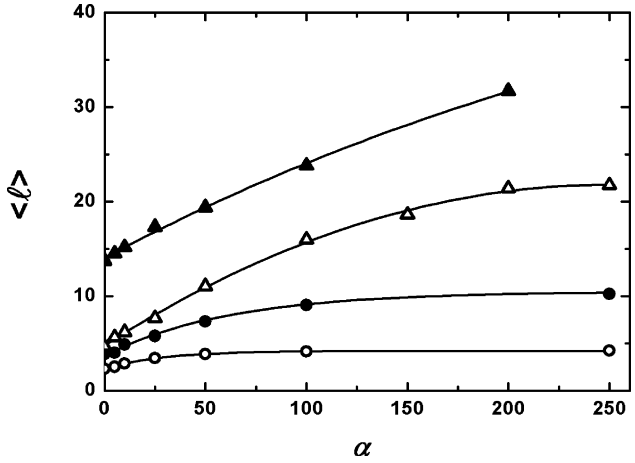

Figure 2. Mean end-to-end distance, $\langle l \rangle$, at the different α values considered in the simulations for chains of length $r = 4$ (○), 8(●), 16 (△), and 32 (▲). The lines are simply guides for the eye.

that minimized the deviation between the measured curve and the Ising curve.

Chain lengths, r, ranging from 4 to 32, were studied, and α values were considered such that the polymers ranged from completely flexible chains to almost stiff rods. For all chains, to increase the number of accepted insertions, Rosenbluth weights[42] were calculated and taken into account in the acceptance criteria for the insertion and removal steps. For flexible chains (defined as those for which the ratio of the bending constant divided by the thermal energy $\alpha/kT < 1$), the Rosenbluth weights were simply obtained as the ratio of the number of unoccupied growth directions divided by the total number of growth directions ($z = 26$). For stiff chains ($\alpha/kT \geq 1$) the bending energy was also included in the calculation of the Rosenbluth weights.

Typical runs consisted of approximately $(50-100) \times 10^6$ equilibration and $(0.2-1) \times 10^9$ production steps requiring between 1 and 8 CPU hours (depending of system density and size) on Intel Pentium IV 1.8 GHz processors. For this work, 80% of the Monte Carlo moves performed were insertions and deletions and the remaining were reptations. The latter are useful for sampling configurations in dense systems, especially for long chains.

For a given chain length and stiffness parameter, a few preliminary short runs were performed in the critical region. Histograms obtained from these runs were used to get preliminary estimates of critical temperatures, densities, and chemical potentials according to the mixed-field finite scaling analysis described above. These critical parameters were then used for a longer, more accurate, run and a better match to the universal Ising distribution. Figure 1 shows the agreement that was obtained between the simulation results and the universal Ising distribution.

To obtain the phase envelope, as described in detail in previous work,[21,30] at least four additional simulations were performed at temperatures one or two T^* units lower than T_c^* and chemical potentials suitable for sampling alternatively the dense and the dilute phase. As previously done,[30] the densities φ_1 and φ_2 respectively of the coexisting dense and dilute phases, obtained from the histogram reweighting procedures at arbitrary temperatures, T^*, within the actual temperature range used in the simulations, were used along with the calculated critical parameters, T_c^* and φ_c, to calculate the coexistence lines by a fitting procedure of the equations:[21]

$$^1/_2(\varphi_1 + \varphi_2) - \varphi_c = A\tau^\mu \tag{6}$$

$$\varphi_1 - \varphi_2 = \tau^\beta(B + B_1\tau^\theta) \tag{7}$$

where

$$\tau = \frac{T_c - T}{T_c} \tag{8}$$

and $\beta = 0.326$, $\mu = 0.9$, and $\theta = 0.54$.[27] A, B, and B_1 were used as adjustable parameters.

In all cases the effect of finite sizes was investigated by using simulations boxes of different dimensions L.

Results and Discussion

Phase diagrams for chains with $r = 4$, 8, 16, and 32 were calculated following the procedure described in the previous section at different values of the stiffness parameter α. The α values were chosen in such a way to gradually increase the chain stiffness and thereby change the average chain conformations from fully flexible chains to semiflexible all the way to stiff rods. An estimate of the chain stiffness can be obtained from the mean end-to-end distance, $\langle l \rangle$, calculated for representative dilute configurations as

$$\langle l \rangle = \frac{1}{n}\sum^{n}\sqrt{(x_r - x_l)^2 + (y_r - y_l)^2 + (z_r - z_l)^2} \tag{9}$$

where n is the number of different chains in the considered configuration and x, y, z are the lattice coordinates of the last (r) and first (l) beads, respectively, in each chain. In Figure 2, the values of $\langle l \rangle$ vs α are shown for the chain lengths studied. The values were calculated at temperatures $T^* = 0.95T_c^*$ for each chain length. It can be observed that, on increasing the stiffness parameter, the chains become elongated and their length approaches a constant value. The lengths of completely extended chains consisting of r beads and oriented along the (0,0,1), (0,1,1), and (1,1,1) directions

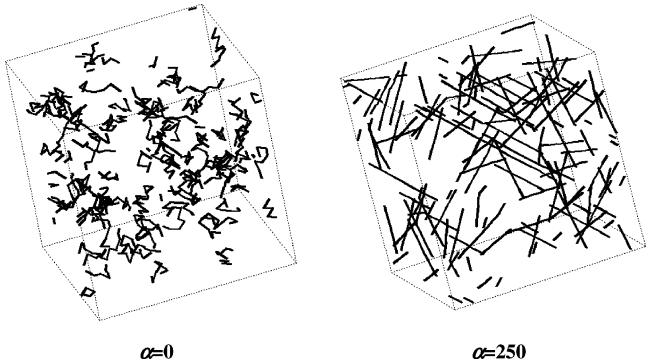

Figure 3. Sample configurations for chains of length $r = 8$ at the two extreme α values: $\alpha = 0$ (left) and $\alpha = 250$ (right). Both configurations were obtained at the following conditions: $L = 30$, $T^* = 0.95T_c^*$, and approximately 100 chains.

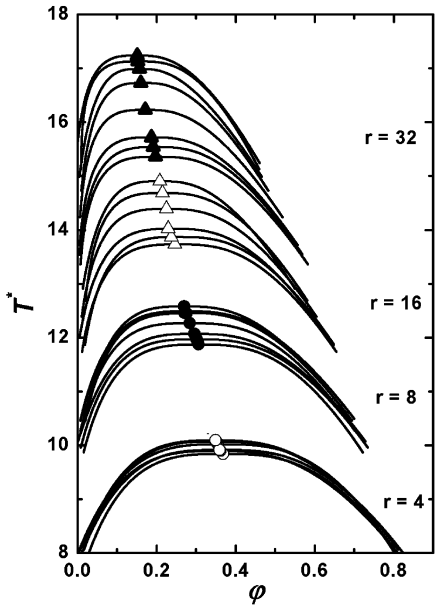

Figure 4. Reduced temperatures, T^*, vs volume fractions, φ, at coexistence. The lines represent fits of Monte Carlo results to scaling relationships (see text). The curves for $r = 4$ and $r = 8$ correspond, from bottom to top, to $\alpha = 0$, 5, 10, 25, 50, 100, 250. For $r = 16$ the curves correspond, from bottom to top, to $\alpha = 0$, 5, 10, 25, 50, 100, 150. For $r = 32$ the curves correspond, from bottom to top, to $\alpha = 0$, 5, 10, 25, 50, 100, 150, 200. Critical points for $r = 4$ (○), 8 (●), 16 (△), and 32 (▲) were calculated as explained in the text.

are $(r - 1)$, $(r - 1)\sqrt{2}$, and $(r - 1)\sqrt{3}$ lattice units, respectively. Assuming that all 26 possible orientations are equally likely, the resulting effective length, l_{fe}, of a fully extended chain can be considered as the average of the three possible lengths. These values are $l_{fe} = 4.2$ for $r = 4$, $l_{fe} = 9.9$ for $r = 8$, $l_{fe} = 21.2$ for $r = 16$, and $l_{fe} = 43.9$ for $r = 32$. As shown in Figure 2, for shorter chains the predicted fully extended lengths were reached.

Furthermore, in Figure 3 are shown typical configurations obtained from chains with $r = 8$ at the two extreme α values in order to demonstrate the induced changes in the conformations.

The overall phase results, for all the studied homopolymer architectures, are shown in Figure 4. The statistical uncertainties on all critical temperatures were estimated by averaging results from four independent simulations performed at the same conditions and different initial seeds of the random sequence. In one representative case ($r = 8$, $\alpha = 250$, $L = 20$), the phase diagram was calculated by using four independent sets of simulations at the same conditions and, again, using different initial seeds of the random sequences. Maximum observed differences in the calculated coexistence points were of the order of 0.5%. The possible presence of finite size effects was checked by using cells of different dimensions (see Table 1). As far as coexistence densities are concerned, the observed differences were always within statistical uncertainties. The continuous lines in the above figure represent results from the fit of eqs 6 and 7.

In all phase diagrams of short chains, away from the critical point, little effects of chain flexibility was observed on coexistence densities. The effect of flexibility is more noticeable for longer chains. The trend high-

Table 1. Critical Temperatures, T_c^*, Densities, φ_c, and Chemical Potentials, μ_c, for Chains T_r at Different Values of the Stiffness Parameter α[a]

α	L	T_c	φ_c	μ_c
		$r = 4$		
0	15	9.85(1)	0.368(3)	−40.62(1)
5	10	9.88(1)	0.365(3)	−31.79(1)
5	15	9.90(1)	0.363(1)	−31.80 (1)
10	10	9.92(1)	0.362(1)	−24.42(1)
10	15	9.94(1)	0.360(1)	−24.43(1)
25	10	9.997(3)	0.357(1)	−9.063(8)
25	15	10.02(1)	0.355(1)	−9.049(5)
50	10	10.040(1)	0.353(1)	4.560(2)
50	15	10.068(3)	0.351(1)	4.615(7)
100	15	10.071(6)	0.351(2)	16.86(2)
250	15	10.07(1)	0.351(3)	23.83(1)
		$r = 8$		
0	15	11.873(4)	0.307(1)	−60.46(1)
5	10	11.96(1)	0.304(4)	−33.693(2)
5	15	11.97(1)	0.3009(9)	−33.70(1)
5	20	11.98(1)	0.3369(8)	−33.69(1)
10	10	12.059(3)	0.2959 (3)	−10.49(1)
10	15	12.070(2)	0.2957(9)	−10.49(1)
10	20	12.08(1)	0.295(1)	−10.491(4)
25	10	12.27(1)	0.2865(9)	41.41(2)
25	15	12.305(1)	0.2831(9)	41.50(1)
25	20	12.32 (5)	0.281(1)	41.54(1)
50	10	12.10(1)	0.2812(1)	91.64(6)
50	15	12.46(3)	0.276(1)	92.00(2)
50	20	12.49(1)	0.274(2)	92.17(5)
100	20	12.49(1)	0.270(3)	141.3(1)
250	15	12.45(1)	0.276(1)	352.5(2)
250	20	12.51(1)	0.274(2)	354.7(3)
250	25	12.53(1)	0.2778(1)	355.2(3)
		$r = 16$		
0	15	13.732(3)	0.2545(1)	−82.62(1)
5	15	13.870(1)	0.246(7)	−19.57(1)
5	20	13.880(1)	0.2445(7)	−19.56(1)
10	15	14.022(2)	0.2397(7)	36.38(1)
10	20	14.03(8)	0.238(2)	36.38(1)
25	15	14.396(1)	0.2243(1)	167.66(6)
25	20	14.42(1)	0.222(1)	167.84(1)
50	15	14.69(1)	0.216(1)	304.36(1)
50	20	14.74(4)	0.211(6)	305.1(1)
100	20	14.91(1)	0.208(1)	445.5(1)
150	20	14.92(1)	0.207(2)	516.0(1)
		$r = 32$		
0	30	15.36(1)	0.201(4)	−104.2(1)
5	30	15.54(3)	0.195(5)	31.93(3)
10	30	15.72(1)	0.187(8)	154.5(1)
25	30	16.23(2)	0.171(3)	451.4(2)
50	30	16.73(1)	0.160(1)	778.2(2)
100	30	16.99(1)	0.157(1)	1127(1)
150	30	17.13(1)	0.155(1)	1313(1)

[a] Data obtained from GCMC simulations performed in cubic cells of different dimensions L. Figures in parentheses represent uncertainties in the last quoted digit.

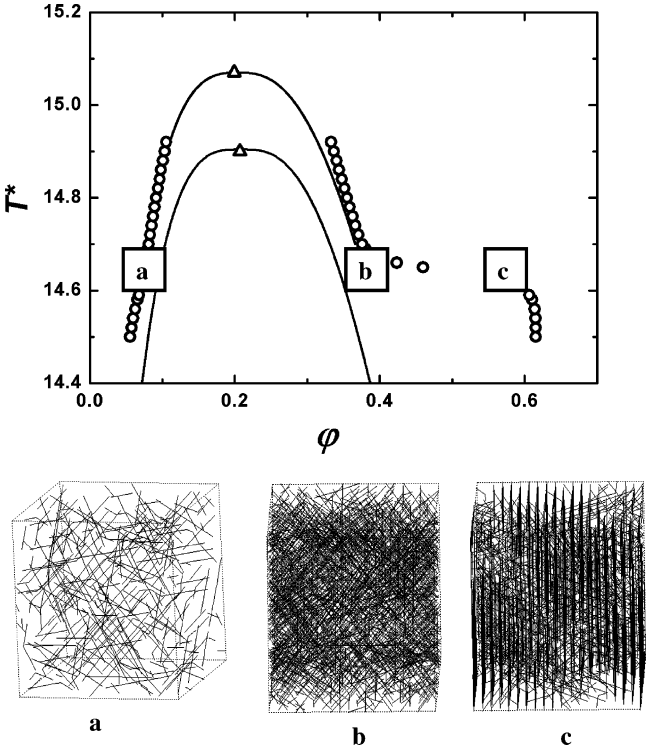

Figure 5. Reduced temperatures, T^*, vs volume fractions, φ, at coexistence for $r = 16$, $\alpha = 150$ (lower curve), and $\alpha = 200$ (top curve). The lines represent fits of Monte Carlo results to scaling relationship (eqs 6 and 7). Critical points, calculated as in Figure 4, are indicated by (△). For the case $\alpha = 200$, actual simulation results (○) and sample configurations, obtained in the indicated positions of the phase diagram, demonstrate the formation of a very dense ordered phase.

lighted here confirms the theoretical predictions[33] and previous simulation data.[38] For longer homopolymer ($r = 16$ and $r = 32$), at high α values the formation of very dense, ordered phases was observed. This is consistent with previous findings for other similar systems.[35] For example, in Figure 5 the calculated phase diagrams for $r = 16$ are compared at $\alpha = 150$ and $\alpha = 200$. It can be seen that, on increasing the rigidity in a long chain, the temperature range where the dilute−dense equilibrium exists decreases. This behavior is a direct consequence of the stabilization of an ordered very dense phase with respect to the disordered liquidlike phase, as the α value is increased. The isotropic−nematic transition is expected for longer and rigid chains because of their higher orientational order with respect to short ones, as previous work has pointed out.[34] Work is in progress to describe this phenomenon in detail.

For completely flexible chains ($\alpha = 0$), as previously found,[21] on increasing the chain length, T_c^* increases and φ_c decreases. The same behavior is observed, for a given chain length, when the chain becomes stiffer, and this is more evident for longer chains. This is in agreement with previous Monte Carlo simulation results[38] concerning a model of linear three-center and five-center rigid and flexible Lennard-Jones chain molecules in which an increase in the critical temperatures of the linear rigid chains with respect to their flexible counterparts was observed. The opposite trend found by Sheng et al.,[30] i.e., lower critical temperatures for rigid chains, is probably attributable to the different potentials used for rigid and flexible chains. For rigid chains, a torsional potential for the dihedral angles and a bond bending potential were used whereas Lennard-Jones interactions were assumed in the case of fully flexible chains.[30] Therefore, the two models differed not just for the introduction of the effect of flexibility but also for the presence of long-range interactions. When just changes of rigidity are considered, the current results demonstrate that the critical temperature of stiff chains is higher than that of the flexible counterparts.

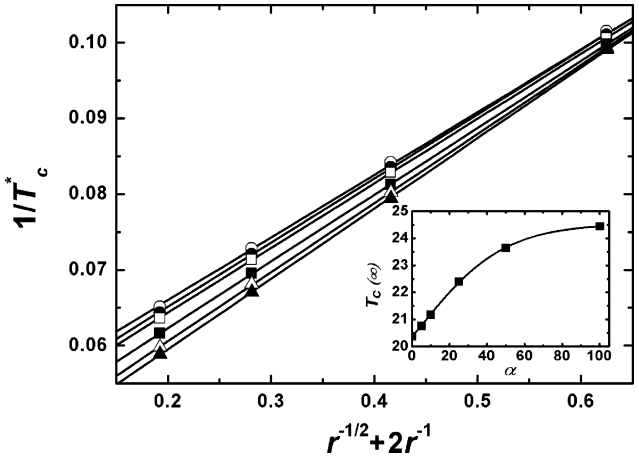

Figure 6. Scaling of critical temperature with chain length (eq 10) at $\alpha = 0$ (○), 5 (●), 10 (□), 25 (■), 50 (△), and 100 (▲). Infinite chain length critical temperatures, obtained from the intercepts of linear fits through the points, are shown in the inset.

Table 2. Infinite Chain Length Critical Temperature, T_c^*, Entropy Parameter ψ, and Exponents x_1 and x_2 for Different Values of the Stiffness Parameter α

α	$T_c^*(\infty)$	ψ	x_1	x_2
0	20.37	0.58	0.11	0.29
5	20.76	0.57	0.11	0.30
10	21.18	0.55	0.13	0.31
25	22.40	0.51	0.16	0.35
50	23.64	0.46	0.22	0.38
100	24.44	0.44	0.23	0.39

Calculated critical temperatures are also plotted as functions of chain length in Figure 6. We have plotted $1/T_c^*$ vs $1/r^{1/2} + {}^1/_2r$, as suggested by the Shultz−Flory relationship:

$$\frac{1}{T_c^*} = \frac{1}{T_c^*(\infty)}\left\{1 + \frac{1}{\psi}\left(\frac{1}{\sqrt{r}} + \frac{1}{2r}\right)\right\} \qquad (10)$$

where $T_c^*(\infty)$ is the infinite chain length critical temperature and ψ, the entropy parameter, is related to the Flory−Huggins entropic term, χ_S, by

$$\chi_S = R\psi\varphi_2^2 \qquad (11)$$

with R being the universal gas constant and φ_2 the volume fraction of the polymer-rich phase.

Estimates of $T_c^*(\infty)$, at different α values, obtained from linear regression of the data of Figure 6, are reported in Table 2. Despite the rather short chain lengths considered and the consequent limited number of data points used in the above fit, a few general conclusions can be drawn. For $\alpha = 0$, the currently obtained value, $T_c^*(\infty) = 20.37$, is in satisfactory agreement with values previously obtained[18,21] ($T_c^*(\infty) = 20.4$ and 20.85, respectively) by considering much longer chain lengths. In agreement with a previous suggestion,[38] the $T_c^*(\infty)$ values gradually increase with α, as

shown in the inset of Figure 6, and tend to level off at relatively large α values.

From Figure 6 it can be seen that, on increasing α, the slope of the linear trends increases. According to eq 10, the slope of these lines is given by $1/[T_c^*(\infty)\psi]$, and therefore, given the $T_c^*(\infty)$ calculated from the intercepts, the ψ values can be obtained and are also reported in Table 2. Needless to say, given the very short chains considered, this analysis is rather crude. However, from a qualitative point of view, since both the slopes of the lines and the values of $T_c^*(\infty)$ increase on increasing α, the entropy parameter, ψ, must decrease for stiffer chains. At the critical temperature, $\varphi_2 = \varphi_c$ is smaller for stiffer chains (see Table 1), and therefore, according to eq 11, χ_S becomes smaller on increasing the stiffness of the chains. This conclusion is consistent with the formation of a more ordered dense phase when stiff rods are packed.

It has been pointed out already that the phase diagrams of Figure 4 indicate that, at a given temperature, an increase in chain stiffness is likely to induce a phase separation phenomenon. For example, a polymer solution constituted by completely flexible chains ($\alpha = 0$) and at T^* values slightly above T_c^* will be homogeneous. However, the same solution, at the same temperature, will phase separate as the parameter α is increased. This is equivalent to saying that the change in chemical potential related to the chain−solvent mixing process becomes less negative. This is consistent with the decreasing entropic term and, also, with an enthalpic term becoming less positive due to the increase in the number of favorable polymer−polymer interactions present when the chains become stiffer.

Other important scaling relationships that can be used to verify the effect of changes in chain conformations are

$$\varphi_c = \frac{1}{1 + r^{-x_2}} \tag{12}$$

and

$$\varphi_1(r,T) - \varphi_2(r,T) \propto r^{-x_1}(1 - T^*/T_c^*(r))^{\beta} \tag{13}$$

From eqs 12 and 13 the x_1 and x_2 exponents can be obtained for all α values and are also reported in Table 2. The Flory−Huggins theory predicts a value of $x_2 = 0.5$ in the limit of infinite chain length. Other experimental[1,5] and modeling[14,22,24,30] studies for long chains have obtained $x_2 = 0.36-0.40$, and there is still some discussion (see for example ref 22) as to what the actual value of x_2 should be. In this work (see Table 2), considering rather short chain lengths, values of x_2 close to literature results were only obtained for the stiffer chains. The same applies to the x_1 exponents which converge to the predicted Flory−Huggins value ($x_1 = 0.25$) only for large values of α. Overall, the above observations suggest that, as it is reasonable to think, making a polymer chain stiffer is equivalent to making it longer.

Conclusions

In this work, lattice GCMC simulations assisted by histogram reweighting techniques and combined with mixed-field finite scaling concepts were used to predict the effect of progressively stiffening the chain backbone on the phase behavior of short cubic lattice chains with 4−32 segments. Longer and/or stiffer chains were not considered in the present work because of the impending formation of very dense ordered phases.

For fully flexible chains, calculated critical parameters were in excellent agreement with previous computer simulation results and theoretical predictions indicating a shift to higher critical temperatures and lower critical densities on increasing the chain length. The same trend was observed, for a given chain length, on increasing the stiffness parameter. It was found that phase envelopes of flexible chains fell below and within the rigid counterparts. In agreement with previous findings, the above observations confirm that, when just changes in flexibility are considered, stiffening the chain backbone is equivalent to increasing its length. Although it is simple to verify that the above conclusions are consistent with experimental findings by comparing critical parameters of, say, increasingly longer hydrocarbons molecules,[1,5] the same is not true when one wants to consider the effect of chain flexibility since, in real systems, stiffening a hydrocarbon chain of a given length always implies also changes in the intermolecular potential. Simulations afford the advantage of isolating individual contributions to the macroscopic behavior.

Analysis of the results indicates that the entropic contribution to the mixing process is smaller when the chains become stiff. This conclusion is consistent with the formation of a more ordered dense phase when stiff rods are packed.

Overall, by analyzing the results under different perspectives, it is clear that an increase in the stiffness of the chain backbone is equivalent to an increase in chain length since both effects contribute to increase the number of favorable polymer−polymer interactions. Further studies are in progress to clarify in detail the microscopic mechanisms involved in the formation of dense ordered phases. It is evident from the present preliminary observations on the formation of dense, ordered (solidlike) phases that there is a connection between the degree of chain stiffness and the range of existence of the isotropic liquid phase in agreement with previous studies[36,38] on fully flexible and stiff chains. Our present results indicate that, for a given chain length, on increasing the chain stiffness the dense ordered phase will form below a certain temperature. For the shorter chains here investigated, this temperature is presumably well below the critical temperature, and therefore, no solidlike phase was observed. On the contrary, for longer chains, we could not increase the stiffness parameter such as to obtain rigid rods because the solid like phase would form in the immediate vicinity of the critical region. In future work it is our intention to vary progressively chain length and flexibility in order to elucidate the details of the interplay between the degree of chain stiffness and the shape of the resulting phase diagram.

Acknowledgment. Financial support for this work has been provided by Università di Palermo (grants ex 60% to M.A.F.), the Department of Energy, Office of Basic Energy Sciences (through Grant No. DE-FG02-01ER15121 to A.Z.P.), and ACS−PRF (Grant 38165-AC9 to A.Z.P.). This work was planned and partially performed during visits by M.A.F. and V.F. to Princeton University. The above are grateful to A.Z.P. for making these visits possible and for making computational facilities available.

References and Notes

(1) Dobashi, T.; Nakata, M.; Kaneko, M. *J. Chem. Phys.* **1980**, *72*, 6685.
(2) Koningsveld, R.; Onclin, M. H.; Kleintjens, L. A. In *Polymer Compatibility and Incompatibility: Principles and Practices*; MMI Press Symposium Series; Šolc, K., Ed.; Harwood Academic Publisher: Chichester, 1982, Vol. 2.
(3) Šolc, K.; Stockmayer, W. H.; Lipson, J. E.; Koningsveld, R. In *Multiphase Macromolecular Systems*; Culbertson, B. M., Ed.; Plenum Publishing Corp: Langhorne, PA, 1989.
(4) Kirby, C. F.; McHugh, M. A. *Chem. Rev.* **1999**, *99*, 565.
(5) Koningsveld, R.; Stockmayer, W. H.; Nies, E. *Polymer Phase Diagrams*; Oxford University Press: New York, 2001.
(6) Enders, S.; Wolf, B. A.; Binder, K. *J. Chem. Phys.* **1995**, *103*, 3809.
(7) Shinozaki, K.; Tan, T. V.; Saito, Y.; Nose, T. *Polymer* **1982**, *23*, 728.
(8) Chu, B.; Wang, Z. *Macromolecules* **1988**, *21*, 2283.
(9) Sanchez, I. C. *J. Phys. Chem.* **1989**, *93*, 6983.
(10) Xia, K.-Q.; Franck, C.; Widom, B. *J. Chem. Phys.* **1992**, *97*, 1446.
(11) Flory, P. J. *Principles of Polymer Chemistry*; Cornell University Press: Ithaca, NY, 1953; Chapter XIII.
(12) Wertheim, M. S. *J. Chem. Phys.* **1986**, *85*, 2929.
(13) de Gennes, P.-G. *Scaling Concepts in Polymer Physics*; Cornell University Press: Ithaca, NY, 1979; Chapter IV, Sect. 3.
(14) Widom, B. *Physica A* **1993**, *194*, 532.
(15) Yu, M.; Liu, Q. *Macromolecules* **1996**, *29*, 6928.
(16) Frauenkron, H.; Grassberger, P. *J. Chem. Phys.* **1997**, *107*, 9599.
(17) Madden, W. G.; Pesci, A. I.; Freed, K. F. *Macromolecules* **1990**, *23*, 1181.
(18) Mackie, A. D.; Panagiotopoulos, A. Z.; Kumar, S. K. *J. Chem. Phys.* **1995**, *102*, 1014.
(19) Smit, B.; Karaborni, S.; Siepmann, J. I. *J. Chem. Phys.* **1995**, *102*, 2126.
(20) Wilding, N. B.; Müller, M.; Binder, K. *J. Chem. Phys.* **1996**, *105*, 802.
(21) Panagiotopoulos, A. Z.; Wong, V.; Floriano, M. A. *Macromolecules* **1998**, *31*, 912.
(22) Yan, Q.; de Pablo, J. J. *J. Chem. Phys.* **2000**, *113*, 5954.
(23) Wijmans, C. M.; Smit, B.; Groot, R. D. *J. Chem. Phys.* **2001**, *114*, 7644.
(24) Indrakanti, A.; Maranas, J. K.; Panagiotopoulos, A. Z.; Kumar, S. K. *Macromolecules* **2001**, *34*, 8596.
(25) Pamies, J. C.; Vega, L. F. *Mol. Phys.* **2002**, *100*, 2519.
(26) Honnell, K. G.; Curro, J. G.; Schweizer, K. S. *Macromolecules* **1990**, *23*, 3496.
(27) Vega, C.; Paras, E. P. A.; Monson, P. A. *J. Chem. Phys.* **1992**, *96*, 9060.
(28) Wojciechowski, K. W.; Branca, A. C.; Frenkel, D. *Physica A* **1993**, *196*, 519.
(29) Yethiraj, A.; Kumar, S.; Hariharan, A.; Schweizer, K. S. *J. Chem. Phys.* **1994**, *100*, 4691.
(30) Sheng, Y.-J.; Panagiotopoulos, A. Z.; Kumar, S. K. *Macromolecules* **1996**, *29*, 4444.
(31) Escobedo, F. A.; de Pablo, J. J. *Mol. Phys.* **1996**, *87*, 347.
(32) Perera, A.; Sokolić, F. *Mol. Phys.* **1996**, *88*, 543.
(33) Blas, F. J.; Vega, L. F. *Mol. Phys.* **1997**, *92*, 135.
(34) Fynewever, H.; Yethiraj, A. *J. Chem. Phys.* **1998**, *108*, 1636.
(35) Polson, J. M.; Frenkel, D. *J. Chem. Phys.* **1998**, *109*, 318.
(36) Ivanov, V. A.; Stukan, M. R.; Müller, M.; Paul, W.; Binder, K. *J. Chem. Phys.* **2003**, *118*, 10333.
(37) Lü, X.; Kindt, J. T. *J. Chem. Phys.* **2004**, *120*, 10328.
(38) Galindo, A.; Vega, C.; Sanz, E.; MacDowell, L. G.; de Mighel, E.; Blas, F. J. *J. Chem. Phys.* **2004**, *120*, 3957.
(39) Ferrenberg, A. M.; Swendsen, R. H. *Phys. Rev. Lett.* **1988**, *61*, 2635.
(40) Wilding, N. B.; Bruce, A. D. *J. Phys.: Condens. Matter* **1992**, *4*, 3087. Wilding, N. B. *Phys. Rev. E* **1995**, *52*, 602.
(41) Kim, Y. C.; Fisher, M. E. *J. Phys. Chem. B* **2004**, *108*, 6750.
(42) Frenkel, D.; Smit, B. *Understanding Molecular Simulation,* 2nd ed.; Academic Press: London, 2002.

MA047671S